Int J Adv Manuf Technol (2013) 66:1715–1724
DOI 10.1007/s00170-012-4452-1

ORIGINAL ARTICLE

3D metal removal simulation to determine uncut chip thickness, contact length, and surface finish in grinding

Abdalslam Darafon · Andrew Warkentin · Robert Bauer

Received: 14 May 2012 / Accepted: 6 August 2012 / Published online: 6 September 2012

Abstract The two most important geometric parameters that describe the mechanics of grinding are the uncut chip thickness and the contact length. Currently, analytical approaches are used to estimate these parameters. The accuracy of these approaches, however, is limited because they do not take into account the random shape, size, and protrusion height and placement of the abrasive grains around the circumference of the grinding wheel. In this paper, a simulation technique was used to gain new insight into the effect of the stochastic nature of grinding wheels on the geometric properties of the grinding process. The simulator was used to calculate the number of active grains, uncut chip thickness, and contact length for a stochastic wheel model of Radiac Abrasive's WRA-60-J5-V1 grinding wheel. These values were then mapped to every grain on the grinding wheel and used to determine the instantaneous material removal rate of the wheel and workpiece surface finish. There was excellent agreement between the predicted and experimentally measured surface topology of the workpiece. The results suggest that only 10–25 % of the grains on the grinding wheel are active and that the average grinding chip may be as much as ten times thicker and ten times shorter than would be produced by a grinding wheel with a regular arrangement of cutting edges as assumed by existing analytical approaches.

A. Darafon · A. Warkentin (✉) · R. Bauer
Department of Mechanical Engineering, Dalhousie University, Halifax, NS, Canada
e-mail: Andrew.Warkentin@dal.ca

A. Darafon
e-mail: Ab303844@dal.ca

R. Bauer
e-mail: Robert.Bauer@dal.ca

Keywords Grinding simulation · Chip thickness · Contact length · Surface roughness · Metal removal · Active grains

1 Introduction

The grinding process is a cutting operation in which abrasive grains cut the workpiece material into the desired shape. Like all machining methods, the material is removed in a chip formation process—but at a much finer scale. The cutting-tool geometry and its interaction with the workpiece in grinding are not as well defined as in other material removal methods such as turning and milling. A grinding wheel has a multitude of geometrically undefined cutting points which are irregularly distributed on its working surface and which are presented to the workpiece at random orientations and positions. Therefore, there is significant variation in the cutting geometry along the circumference of the wheel. The stochastic nature of grinding wheels makes it difficult to determine fundamental geometric properties of grinding such as the uncut chip thickness and contact length for individual grains. These quantities are essential in order to accurately predict forces, power, temperature, and workpiece surface roughness in grinding.

There has been extensive research conducted into the modeling and simulation of grinding wheel surfaces and the resulting workpiece surface finish as reviewed in Doman et al. [1]. Simulation approaches have attempted to use a model of the grinding wheel topology, process kinematics, and workpiece grit interaction to determine the topology of the workpiece surface. Grinding wheel models generally take into account the grain geometry and distribution on the grinding wheel. The grain geometry has often been approximated by

spheres (Chen and Rowe [2]), cones (Cooper and Lavine [3]), ellipsoids (Hegeman [4]), pyramidal (Chakrabarti et al. [5]), and truncated cones (Warnecke and Zitt [6]), or has been generated from modified basic geometries such as octahedrons, cuboids, and tetrahedrons (Warnecke et al. [6]). Spherical grains are relatively easy to define from the grinding wheel marking information (Doman et al. [1]) while more complex shapes may require difficult grain measurements (Chakrabarti et al. [5]) and consideration of the grain's orientation (Hegeman et al. [4]). The stochastic distribution of the grains in a grinding wheel is usually accomplished in two ways. In the first method, abrasive grits are evenly spaced on the grinding wheel and then randomly moved, as in the case of Chen and Rowe [2] or Hegeman [4]. In the second method, a stochastic distribution is used to place the abrasive grains directly on the grinding wheel, as in the case of Chakrabarti et al. [5]. In either case, care should be taken to ensure that abrasive grains do not overlap and that the grain density is relatively consistent throughout the entire grinding wheel model. Once the wheel model has been defined, the trajectory of each grain must be established. In the case of surface grinding, the trajectories of the grains have a combination of rotational and linear motion. This motion can be expressed exactly as parametric functions of time or approximated by parabolic curves in space as described by Nguyan and Butler [7]. In order to model the interaction of an abrasive grain with the workpiece, a model of the workpiece must be created. The workpiece generally consists of a 2D array of numbers with each number representing the height of the workpiece surface at a particular point (see, for example, the work of Chakrabarti et al. [5] or Nguyan and Butler [7].) The workpiece surface can then be determined by the height of the grain's trajectory as the grain passes over a point on the workpiece. Note that it is possible to incorporate the cutting mechanics of individual grains into the model by modifying the height information recorded in the workpiece array based on a cutting mechanics model as proposed by Nguyan and Butler [7].

Similar to the previously mentioned research, the simulation that will be presented in this paper can be used to predict the surface finish produced by a grinding process. The proposed simulator, however, also has the additional unique ability to calculate the uncut chip thickness and contact length for every cutting edge on a grinding wheel.

2 Background

In the microscale, the uncut chip thickness is the depth that a cutting edge immerses itself in the workpiece material, while the contact length is the distance the grain travels

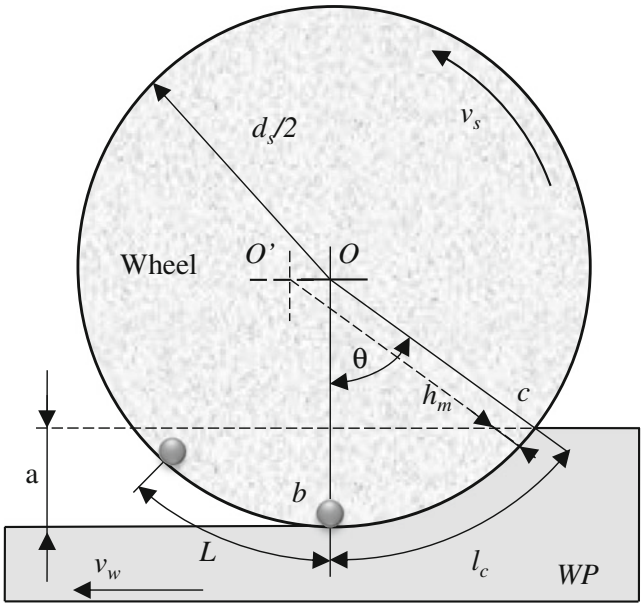

Fig. 1 Geometry of surface grinding

while in contact with the workpiece as illustrated in Fig. 1. A wheel of diameter d_s rotating with a peripheral velocity v_s takes a depth of cut a from the workpiece as it translates at velocity v_w. Penetration of the grinding wheel into the workpiece results in an apparent area of contact where the grinding action occurs. The contact length is indicated by l_c. Neglecting motions and deformations of the wheel and workpiece, the contact length is generally approximated by [8]:

$$l_c = \sqrt{a\, d_s} \tag{1}$$

In order to derive an expression for the uncut chip thickness, the cutting edges (abrasive grains) are assumed to be spaced a distance L around the circumference of the grinding wheel. The paths of the cutting

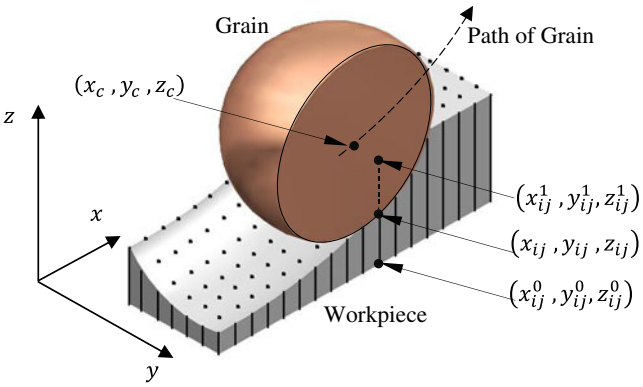

Fig. 2 Metal removal simulation for a single grain

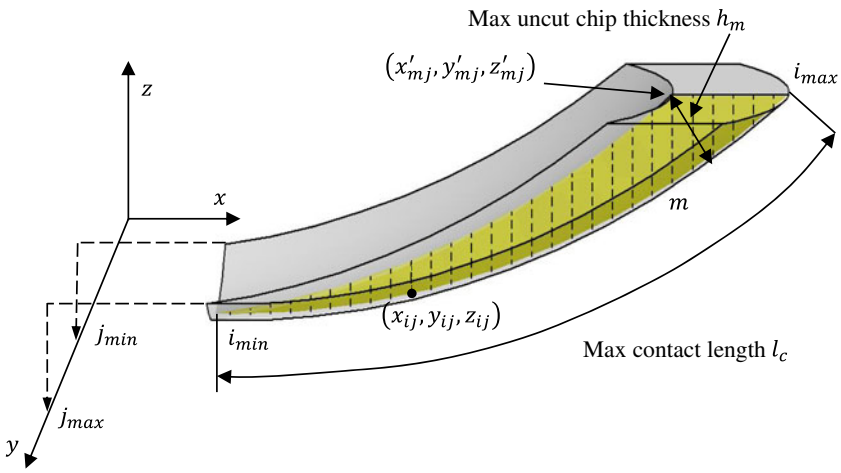

Fig. 3 The uncut chip thickness and contact length on the 3D chip

edges are assumed to be circular arcs. This assumption implies an intermittent motion in which the workpiece remains stationary during an individual cut, and then moves instantaneously by the distance O′O before the next cutting point engages. Using these assumptions, the uncut chip thickness can be calculated by [8]:

$$h_m = 2L\left(\frac{v_w}{v_s}\right)\left(\frac{a}{d_s}\right)^{0.5} \tag{2}$$

3 Method

The proposed 3D grinding metal removal simulator described in this paper is based on the work of Kim [9] which was used to simulate metal removal in surface milling. Kim's method was selected because it is relatively straightforward to implement, computationally efficient, and can easily be adapted to 2D or 3D grinding simulation. In the proposed simulator, the workpiece is represented by a set of evenly spaced vertical line segments distributed in the x–y plane, sometimes referred to as a z-map, and the abrasive grain is represented by a sphere as shown in Fig. 2

The position of each line segment in the array is identified by its i and j indexes. The length of each line segment, in the z-direction, represents the workpiece height. The number of line segments in the x- and y-directions multiplied by the space between the line segments represents the workpiece length and width. The accuracy of the workpiece representation is determined by the spacing of the line segments. Smaller spacing will result in a more accurate but computationally slower model, while larger spacing will result in a less accurate but computationally faster model. In this work, the line segment spacing was 1.0 μm. Each line segment is represented by a 1D parametric equation, which uses a length parameter called f as follows:

$$x_{ij} = x_{ij}^1 - f\left(x_{ij}^1 - x_{ij}^0\right) \tag{3}$$

$$y_{ij} = y_{ij}^1 - f\left(y_{ij}^1 - y_{ij}^0\right) \tag{4}$$

$$z_{ij} = z_{ij}^1 - f\left(z_{ij}^1 - z_{ij}^0\right) \quad [0 \le f \le 1] \tag{5}$$

Note that the orientation of the line segments should be normal to the workpiece surface. This work is focused on

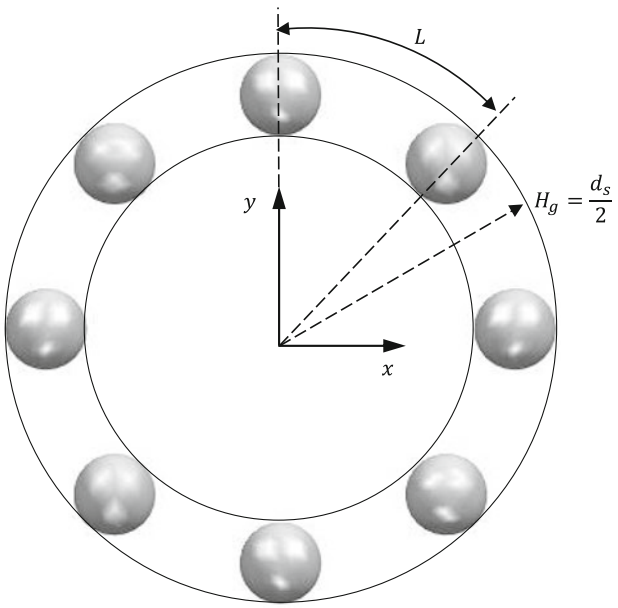

Fig. 4 Illustration of the single-row constant-value model

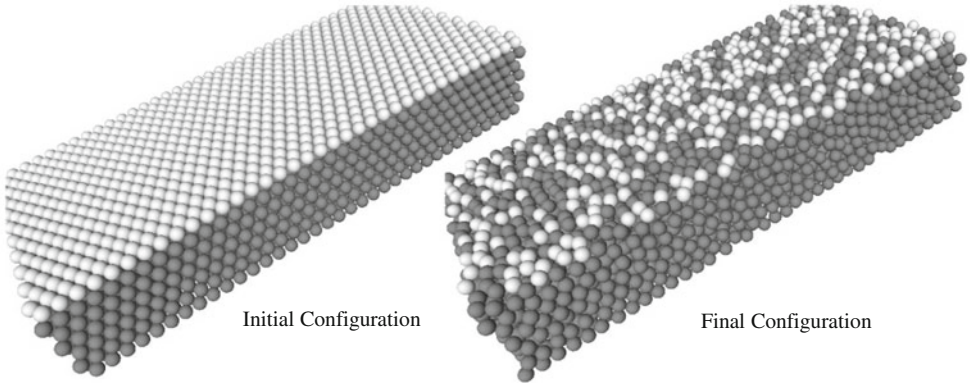

Fig. 5 The stochastic grinding wheel model before and after shaking process

flat surface grinding so the line segments are parallel with the z-axis, $x_{ij}=x_{ij}^{0}=x_{ij}^{1}$ and $y_{ij}=y_{ij}^{0}=y_{ij}^{1}$.

In this work, the grains are assumed to have a spherical shape. Note, however, that with this technique, any grain shape can be modeled. The sphere center (x_c, y_c, and z_c) travels along a trochoidal path, which is a combination of a rotation and a translation as expressed in Eqs. (6), (7), and (8):

$$x_c(t) = v_w t + \frac{d_s}{2}\cos\left(\frac{tv_s}{\frac{d_2}{2}}\right) \tag{6}$$

$$y_c(t) = \text{Constant} \tag{7}$$

$$z_c(t) = \frac{d_s}{2}\sin\left(\frac{tv_s}{\frac{d_2}{2}}\right) \tag{8}$$

where t is the time.

Metal removal is simulated by intersecting the sphere with the line segments at discrete time intervals. The portion of the line segments that are inside the circle (vertical dashed lines in Fig. 2) is removed by adjusting the length of the line segments. Equation (9) describes the sphere, which intersects the line segments:

$$(x-x_c)^2 + (y-y_c)^2 + (z-z_c)^2 = R^2 \tag{9}$$

where R is the sphere radius and x_c, y_c, and z_c is the center of the sphere in the global coordinate system. To define the intersection point between the sphere and each line segment, Eqs. (3), (4), and (5) are substituted into Eq. (9) for x, y, and z to obtain Eq. (10):

$$z_{ij}^2 + 2z_c \quad z_{ij} + k = 0 \tag{10}$$

where

$$k = {z_c}^2 + \left(x_{ij}-x_c\right)^2 + \left(y_{ij}-y_c\right)^2 - R^2$$

By using the quadratic equation, z_{ij} can be determined. The length parameter f is then found by rearranging Eq. (5) in the following manner:

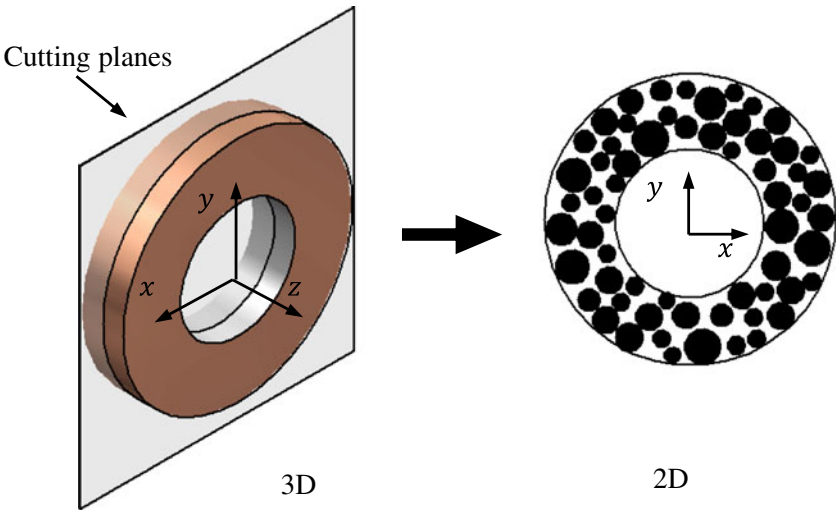

Fig. 6 2D packing density

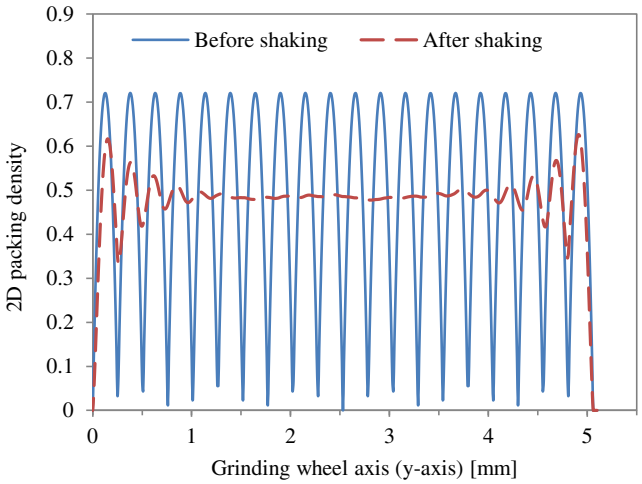

Fig. 7 Packing density in 2D models along the grinding wheel axis

$$f = \frac{z_{ij}^{1} - z_{ij}}{z_{ij}^{1} - z_{ij}^{0}} \tag{11}$$

Note that the length parameter f can be one of the following cases:

1. f=complex number. No intersection point between the line segment and the sphere at all.
2. $f<0$ or $f>1$. The intersection point is outside the range of interest.
3. $0 \le f \le 1$. The intersection point is inside the range of interest.

Once the length parameter f is obtained with a value of $0 \le f \le 1$, the cut portion is removed by substitution of z_{ij}^{1} with the z_{ij} value that is obtained from Eq. (10).

The uncut chip thickness and contact length can be determined by examining the simulated chip as shown in Fig. 3. The chip consists of a rectangular grid of vertical line segments. The chip is then sliced into a series of planes that are parallel to the x–z plane. Each of these slices is numbered from $j_{\min}$ to $j_{\max}$ using its j index. One of these slices is highlighted in Fig. 3. Each line segment in this slice is numbered from $i_{\min}$ to $i_{\max}$ using its i index. The maximum uncut chip thickness $h_{m\,j}$ can be defined for each slice as the shortest distance between the point $(x'_{m\,j}, y'_{m\,j}, z'_{m\,j})$ shown in Fig. 3 and the bottom vertices of the line segments representing the chip as described by Eq. (12).

$$h_{m_j} = min_{i=i_{\min}\to i_{\max}} \left[\sqrt{(x_{mj} - x_{ij})^2 + (y_{mj} - y_{ij})^2 + (z_{mj} - z_{ij})^2} \right] \tag{12}$$

The maximum uncut chip thickness can then be found by determining the maximum values of the chip thickness for all the slices making up a chip. However, since the chip cross-section is very irregular, this measure of chip thickness was deemed to be a poor measure of the actual chip thickness. An average maximum chip thickness was used instead by finding the average of the maximum uncut chip thicknesses for all cross-section planes as shown in Eq. (13).

$$h_m = \frac{1}{j_{\max} - j_{\min}} \sum_{j=j_{\min}}^{j_{\max}} h_{m_j} \tag{13}$$

The contact length for each cross-section is the summation of the distances between the bottom vertices of successive cut line segments as shown in Eq. (14).

$$l_{c_j} = \sum_{j=j_{\min}}^{j_{\max}} \sqrt{(x_{(i-1)j} - x_{ij})^2 + (y_{(i-1)j} - y_{ij})^2 + (z_{(i-1)j} - z_{ij})^2} \tag{14}$$

Therefore, the average contact length for the chip is:

$$l_c = \frac{1}{j_{\max} - j_{\min}} \sum_{j=j_{\min}}^{j_{\max}} l_{c_j} \tag{15}$$

The proposed simulator was used in conjunction with both a non-stochastic as well as a stochastic wheel model. The non-stochastic model consisted of a single row of uniformly sized grains evenly spaced about the circumference of the grinding wheel as shown in Fig. 4. For the stochastic model the grain size, protrusion height, and spacing were randomly distributed. According to Malkin [8], Eqs. (16) and (17) can be used to calculate the average grain diameter d_g and the grain volume fraction V_g. For this work, the nominal grain diameter, protrusion height, and spacing were determined based on a wheel with a grit number M of 60 and a structure number S of 8.

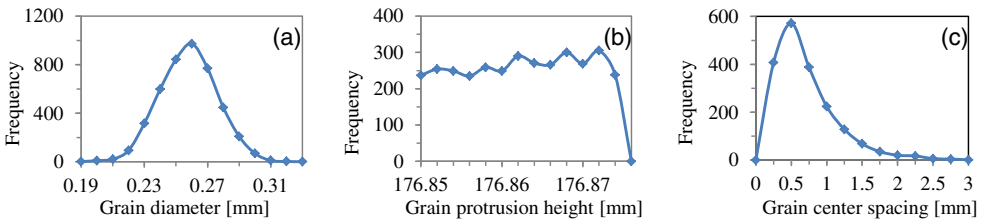

Fig. 8 **a** Grain diameter histogram, **b** grain protrusion height histogram, and **c** grain center spacing histogram for stochastic grinding wheel model

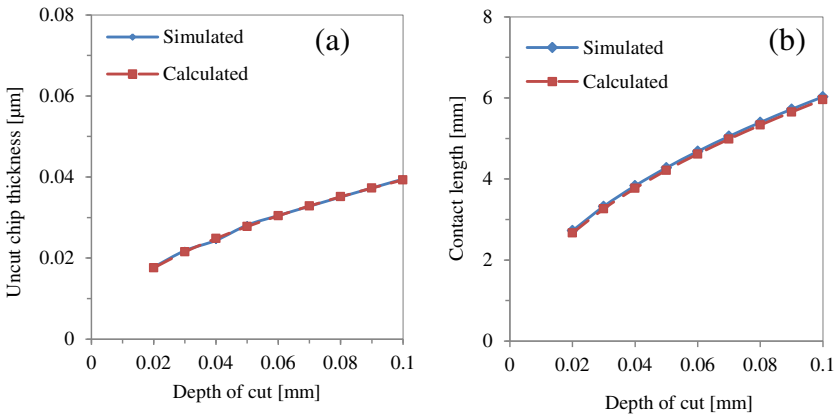

Fig. 9 **a** Simulated and calculated uncut chip thickness vs. the depth of cut for the non-stochastic model. **b** Simulated and calculated contact length vs. the depth of cut for the non-stochastic model

$$d_g = 15.2M^{-1} \tag{16}$$

$$V_g = 0.02(32 - S) \tag{17}$$

For the non-stochastic model, the grinding wheel takes the shape of a torus; therefore, the packing density in this model is the number of grains n times the grain volume V_{grain} divided by the volume of the torus V_t:

$$V_g = \frac{nV_{\text{grain}}}{V_t} = \frac{n\frac{\pi}{6}d_g^2}{\frac{\pi^2}{4}(d_s - d_g)d_g^2} \tag{18}$$

Therefore, the number of grains in the non-stochastic model can be calculated by rewriting Eq. (18) as follows:

$$n = \frac{3}{2}\pi V_g\left(\frac{d_s}{d_g} - 1\right) \tag{19}$$

The grain spacing L can be calculated using Eq. (20).

$$L = \frac{\pi(d_s - d_g)}{n} \tag{20}$$

The stochastic model considered the distribution of grain size, spacing, and protrusion height. The model presented in this paper is a modified version of that proposed by Koshy et al. [10]. To generate the stochastic grinding wheel model, grains with the average diameter were distributed evenly within the wheel volume to achieve a grain packing density as shown in the initial wheel segment in Fig. 5. Subsequently, each grain was randomly moved in the *x*-, *y*-, and *z*-directions. If a grain interfered with another grain or was outside the wheel's boundary, it was moved back until it touched the other grain or the wheel border. This process, called shaking, continued until the grain distribution was as homogenous as possible. A portion of the final wheel is shown in Fig. 5. Since the wheel surface is irregular, a decision had to be made as to whether a grain was on the surface of the wheel or not. In this paper, it was decided that if a grain was within 0.1 grain diameter of the maximum protrusion height then the grain was considered to be on the surface and potentially actively involved in cutting. In Fig. 5, the grains that meet this requirement are colored white, and are considered to be on the wheel surface.

The distribution of grains was assessed in the following manner: A number of parallel cutting planes were intersected with the wheel model, as illustrated in Fig. 6. For each plane the area of all the grains were

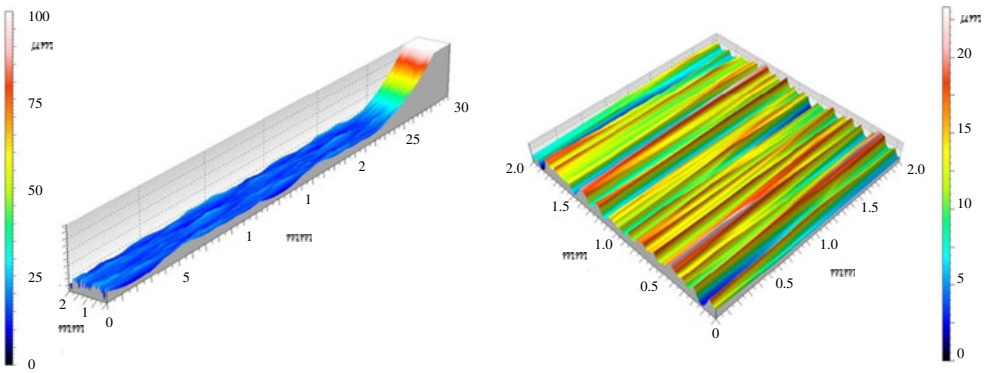

Fig. 10 Sample of simulated workpiece

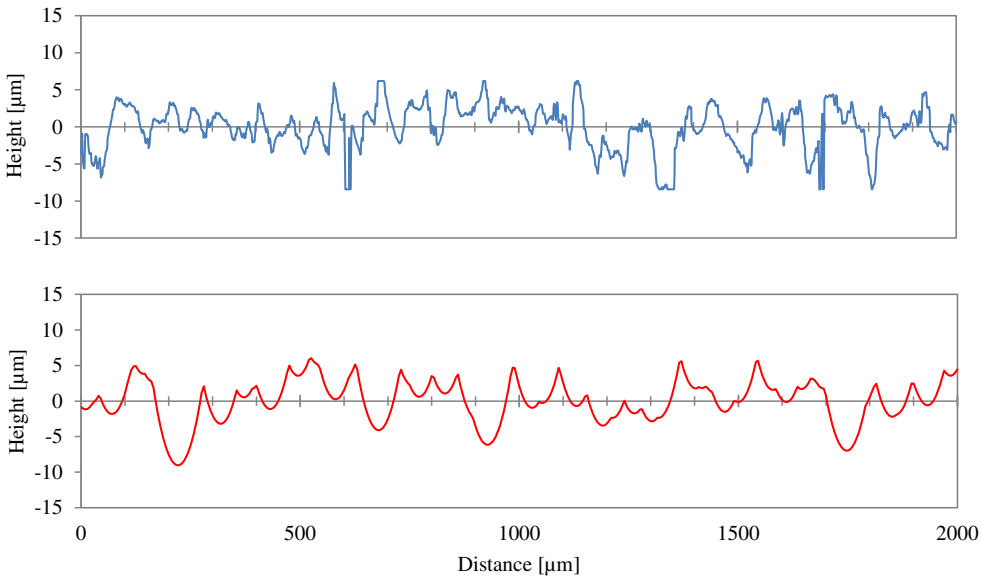

Fig. 11 Experimental (*above*) and the simulated (*below*) profiles of the workpiece

summed up and divided by the total cut area of the wheel.

Figure 7 shows the resulting 2D packing density versus the distance along the y-axis for the stochastic model before and after shaking. Before shaking the packing density varies periodically along the y-axis from 0.0 to approximately 0.72 because of the regular spacing of the grains, but had the anticipated average packing density of 0.48. After shaking, the variation in the packing density is significantly reduced, especially towards the center of the wheel, and the average packing density is still 0.48. Closer to the boundaries, there is still considerable variation in the packing density due to the constraint on grain movement cause by the boundary condition. To mitigate the boundary effect, only the central portion of the stochastic wheel model was used in these metal removal simulations.

After the grains have been shaken, the grain size is adjusted to account for the distribution of grains typically found in grinding wheels. According to Koshy et al. [11] and Hou et al. [12] the distribution of grain sizes for a given nominal grain size usually has a normal distribution. A standard grit number is defined in terms of grain sizes corresponding to five sieves (Malkin [8]). A 60-grit wheel has grains caught on sieves number 46, 54, 60, 70, and 80. Using Eq. (16) and grit numbers 46 and 80, the minimum $d_{g\_\min}$ and maximum $d_{g\_\max}$ grain size were calculated. The standard deviation of the grain diameter was then defined as follows:

$$\delta = \frac{d_{g\_\max} - d_{g\_\min}}{6} \tag{21}$$

Figure 8 shows that the grain diameters used in this research were specified to have a normal distribution. The resulting protrusion height was found to have an approximately uniform distribution and the grain spacing exhibited an approximately gamma distribution.

4 Result and discussion

Simulations of grinding metal removal were carried out using the following parameters for both the non-stochastic

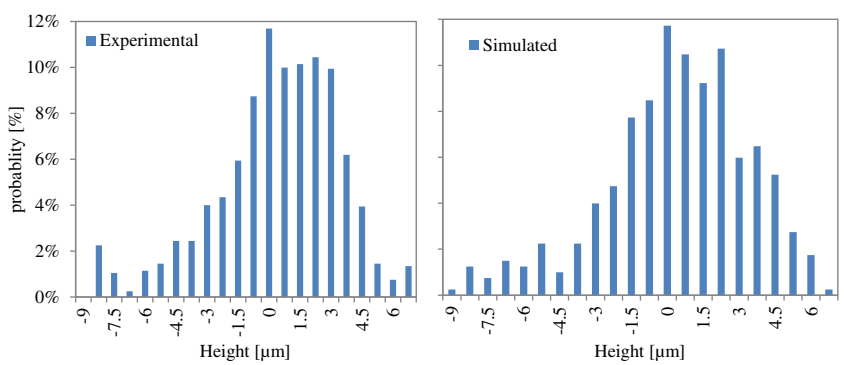

Fig. 12 The histogram of the profile height for the experimental and simulated profiles

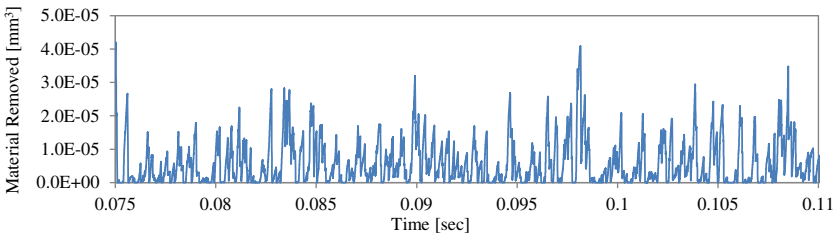

Fig. 13 Simulated material removed vs. time

and stochastic wheel models: depth of cut from 0.02 to 0.1 mm, wheel diameter of 354.04 mm, wheel speed of 30,000 mm/s, and workpiece speed of 100 mm/s.

Figure 9a, b plots the uncut chip thickness and contact length as a function of depth of cut for both the "Simulated" results for the non-stochastic model and the "Calculated" results obtained from Eqs. (1) and (2). The purpose of these figures was to demonstrate that the simulation with the non-stochastic grinding wheel model could replicate the result produced by the analytical approach given the same underlying assumptions that all grains were the same size, had the same protrusion height and were equally spaced around the grinding wheel. These two figures show an excellent agreement between the simulation and analytical results. The differences in the uncut chip thickness and contact length were 0.5 and 1.2 %, respectively, for a depth of cut 0.1 mm, and 1.2 and 2.2 %, respectively, for a depth of cut of 0.02 mm. From this comparison, one can conclude that the proposed simulation is as least as accurate as the analytical approach. The remaining simulated results will use stochastic 3D grinding wheel models to generated surface finish results as well as uncut chip thickness and contact length results.

Next, the simulation using a stochastic wheel model was compared to experimental results. The grinding parameters in the experiment were the same as the grinding parameters used in the simulation. Figure 10 shows the simulated workpiece surface roughness and the resulting surface finish for a depth of cut of 0.09 mm. A Nanovea PS-50 non-contact optical profilometer was used to measure the surface topology of the experimental workpieces. The simulation was terminated when the wheel was fully engaged with the workpiece and had continued to rotate an additional two rotation to make sure that the simulation had reached steady state. The simulated surface was then imported into the same software used to analyze the surface of experimental workpieces to ensure that there were no discrepancies in surface analysis. Figure 11 shows an experimental and simulated profile of the ground surface and Fig. 12 shows the height distribution of the profiles. While the profiles are clearly not identical there are some remarkable similarities. The roughness R_a of the experimental and simulated profiles are 1.9 and 2.1 μm, respectively, and the height distribution appears normally distributed with a range from −9 μm to almost 7 μm. The main difference between the two profiles is that the experimental data appears to have slightly higher frequency content than the simulated data. This discrepancy is likely the result of the fact that real grains may have multiple cutting edges and the simulation does not account for plowing of workpiece material to the sides of the grains. Nevertheless, it should be emphasized that no tuning of the model was required to obtain excellent agreement between the simulated and measured surface roughness values.

The authors believe that the ability to calculate instantaneous metal removal is one of the chief advantages of this approach as it opens the door to better force and power models for grinding. For example, Fig. 13 shows the simulated instantaneous material removal rate for one complete revolution of the 2-mm-wide wheel at a depth of cut of 0.09 mm. The simulated material removal rate is the summation of material removed by the cutting operation divided by the elapsed time. The average simulated MRR is 18 mm^3/s while the material removal rate calculated by multiplying the

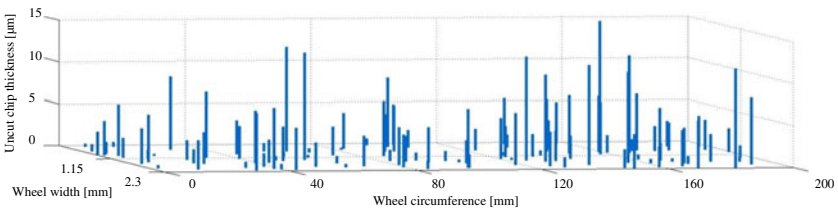

Fig. 14 The simulated uncut chip thickness for every active grain at the depth of cut of 0.09 mm vs. wheel circumference and wheel width

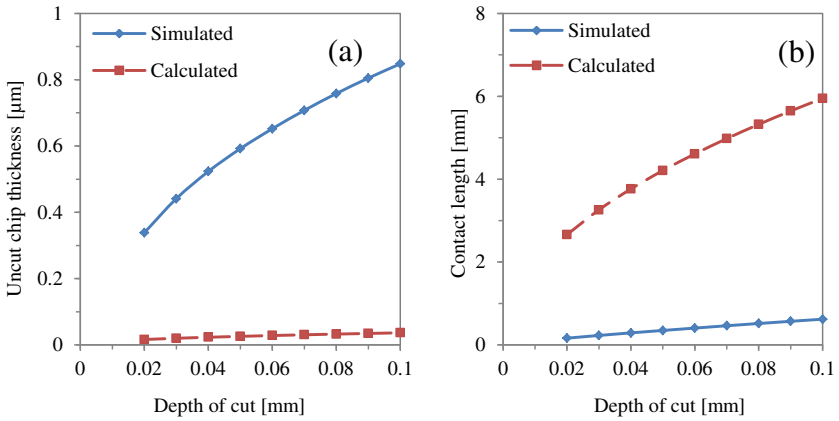

Fig. 15 **a** The Simulated and calculated uncut chip thickness vs. the depth of cut and (**b**) the simulated and calculated contact length vs. the depth of cut for the stochastic model

workpiece width by the depth of cut by the workpiece velocity is also 18 mm^3/s confirming that the bulk metal removal is being simulated correctly.

The simulation also makes it possible to map the uncut chip thickness onto individual cutting edges. Figure 14 shows the uncut chip thickness for every single active grain on a 200-mm section of the wheel surface for a depth of cut of 0.09 mm. From this figure, it is possible to conclude that most of the material removal has been accomplished by relatively few grains. The range of uncut chip thicknesses produced by the stochastic model is huge—the minimum value was 0.0 μm, while the maximum value was 17.9 μm, and the standard deviation was 2.1 μm because only 21.4 % of the grains are actually cutting! This information is critical for those researchers that are conducting finite element simulations of grinding micro-mechanics who need accurate estimates of the uncut chip thickness in order to perform useful simulations.

Figure 15a, b plots the resulting average uncut chip thickness and the average contact length as a function of the depth of cut using simulated results from the stochastic model as well as "Calculated" results from the analytical model. Several observations can be made from these figures. The calculated and the stochastic models behaved in roughly the same manner. As the depth of cut increased, the average uncut chip thickness and the average contact length increased. However, the differences between the simulated and calculated result in the uncut chip thickness are slightly larger than the differences in the contact length. At the depth of cut of 0.1 mm the difference between the simulated and calculated uncut chip thickness and contact length is 95.7 and 89.6 %, respectively.

The difference between the average uncut chip thickness and contact lengths determined via the simulation and the analytical approach can partially be attributed to the difference between the numbers of active grains actually participating in cutting. This difference is quantified by Fig. 16 which shows the percentage of active grains versus the depth of cut for the stochastic model. The percentage of the active grains increases as the depth of cut increases, because more grains that have a small protrusion height participate in the cutting operation. This figure shows that the number of active grains is quite small and ranges from about 11 to 22 %. Given that the number of active grains has a significant effect on the uncut chip thickness and contact length, it make sense to calculate the uncut chip thickness and contact length for the number of active grains for both the simulation and analytical approach as can be seen in Fig. 17. When this correction is made, the discrepancy between the simulated and calculated values drop; however, the simulated results still suggest that the chips are about twice as thick and half as long as the standard analytical calculation would predict. These differences are likely due to the assumption of constant grain spacing and protrusion height made in the analytical solution.

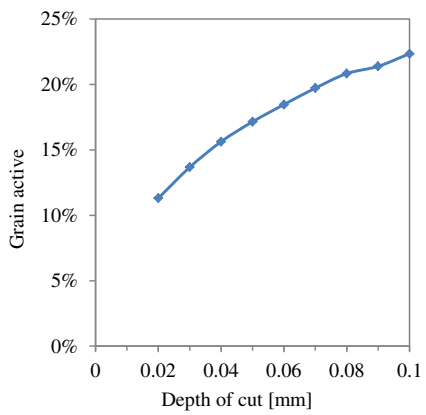

Fig. 16 Grain active vs. depth of cut

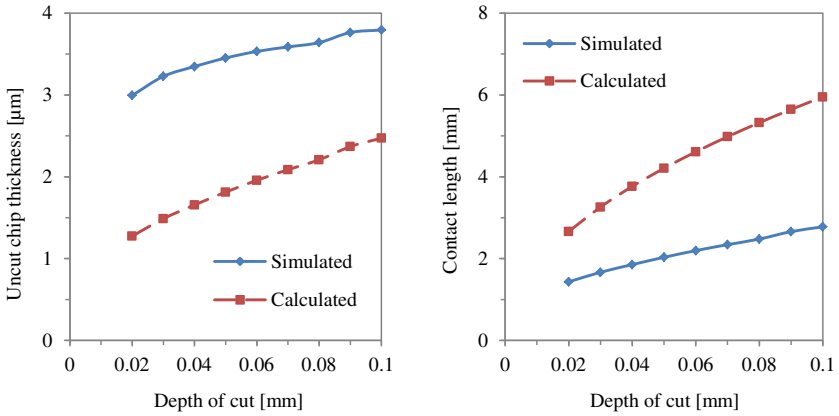

Fig. 17 The effect of the number of active grain on the simulated and calculated result

5 Conclusions

A novel simulation-based method of calculating the uncut chip thickness, the contact length, and surface roughness in grinding is presented based solely on the wheel markings and process parameters, without the use of any tuning parameters. The simulations suggest that the average uncut chip thickness may be ten times larger and the chip length may be ten times shorter than that calculated using conventional analytical models. The simulation also predicted that the number of active grains was between 10 and 25 % of the total grains on the surface of the grinding wheel. Furthermore, grinding experiments were carried out to demonstrate that this novel approach was able to accurately predict the workpiece surface roughness.

The simulation was also shown to be able to calculate instantaneous material removal rates and map chip geometry information to individual grains on the grinding wheel. The ability to calculate instantaneous metal removal is one of the chief advantages of this approach as it opens the door to better force and power models for grinding. The authors feel that this contribution is a significant and useful advancement in grinding technology because it provides new knowledge into better designs of grinding wheels and paves the way towards better mechanistic models of the grinding process as currently exists in machining processes such as milling.

Acknowledgments The authors would like to thank The Natural Sciences and Engineering Research Council of Canada (NSERC) and the Canadian Foundation for Innovation (CFI) for financial support for this work.

References

1. Doman DA, Warkentin A, Bauer R (2006) A survey of recent grinding wheel topography models. Int J Mach Tool Manufact 46:343–352
2. Chen X, Rowe WB (1996) Analysis and simulation of the grinding process. Part I: generation of the grinding wheel surface. Int J Mach Tool Manufact 36:871–882
3. Cooper WL, Lavine AS (2000) Grinding process size effect and kinematics numerical analysis. J Manuf Sci Eng 122:59–69
4. Hegeman JBJW (2000) Fundamentals of grinding: surface conditions of ground materials. Dissertation, University of Groningen
5. Chakrabarti S, Paul S (2008) Numerical modelling of surface topography in superabrasive grinding. Int J Adv Manuf Technol 39:29–38
6. Warnecke G, Zitt U (1998) Kinematic simulation for analyzing and predicting high-performance grinding processes. CIRP Ann Manuf Technol 47:265–270
7. Nguyen TA, Butler DL (2005) Simulation of surface grinding process, part 2: interaction of the abrasive grain with the workpiece. Int J Mach Tool Manuf 45:1329–1336
8. Malkin S (1989) Grinding technology: theory and applications of machining with abrasives. Society of Manufacturing Engineers, Dearborn, Mich
9. Kim C (1995) Verification of NC tool path and manual and automatic editing of NC code. Int J Prod Res 33:659
10. Koshy P, Jain VK, Lal GK (1997) Stochastic simulation approach to modelling diamond wheel topography. Int J Mach Tool Manufact 37:751–761
11. Koshy P, Jain VK, Lal GK (1993) A model for the topography of diamond grinding wheels. Wear 169:237–242
12. Hou ZB, Komanduri R (2003) On the mechanics of the grinding process. Part I. Stochastic nature of the grinding process. Int J Mach Tool Manufact 43:1579–1593